Lawrence Berkeley National Laboratory

Title

A Study of Regional Temperature and Thermohydrological Effects of an Underground Repository for Nuclear Wastes in Hard Rock

Permalink

https://escholarship.org/uc/item/07n712z1

Authors

Wang, J S Y
Tsang, C F
Cook, N G W
et al.

Publication Date

1978-10-01

Copyright Information

A STUDY OF REGIONAL TEMPERATURE AND THERMOHYDROLOGICAL EFFECTS OF AN UNDERGROUND REPOSITORY FOR NUCLEAR WASTES IN HARD ROCK

J. S. Y. Wang, C. F. Tsang,
N. G. W. Cook and P. A. Witherspoon

October 1978

DISCLAIMER

A STUDY OF REGIONAL TEMPERATURE AND THERMOHYDROLOGICAL EFFECTS OF AN

UNDERGROUND REPOSITORY FOR NUCLEAR WASTES IN HARD ROCK[*]

J.S.Y. Wang, C.F. Tsang, N.G.W. Cook and P.A. Witherspoon

Earth Sciences Division, Lawrence Berkeley Laboratory,

University of California, Berkeley, California 94720

ABSTRACT

Heat released by the radioactive decay of nuclear wastes in an underground repository causes a long-term thermal disturbance in the rock mass containing it. The nature of this disturbance for a planar repository 3000 m in diameter at a depth of 500 m below surface is investigated for various waste forms. The effects of changes in the density and viscosity of groundwater caused by the temperature changes on the flow through a simple model of a vertical fracture connected to a horizontal fracture in a rock mass is evaluated. It is concluded that different waste forms and periods before burial have significant effects on the thermal disturbance and that buoyant groundwater flow is a function of both the vertical and horizontal fracture transmissivities, as well as the changes in temperature. Loaded initially with a power density of 10 W/m^2 of spent fuel assemblies 10 years after discharge from a reactor, the maximum increase in temperature of the repository in granite is about $50^\circ C$ and the epicentral thermal gradient about $70^\circ C/km$.

INTRODUCTION

Significant quantities of nuclear wastes exist already and continue to be produced (Department of Energy, 1978). At present, most of these wastes are stored in near surface facilities. Although every precaution is taken to protect man and the environment from the potential hazard posed by these wastes, near surface storage is not regarded as a satisfactory long term proposition. Disposal of the nuclear wastes by deep burial in suitable geologic formations is generally favored (Interagency Review Group, 1978). The principal attraction of disposal by deep burial is that it provides a high degree of physical isolation of the nuclear waste from the biosphere. The principal concern of deep burial is that at no stage should toxic components of these wastes find their way back to the biosphere at levels which are not completely harmless.

A wealth of scientific knowledge and engineering experience exists concerning the excavation of underground openings in a wide variety of geologic media. Unfortunately no comparable experience exists concerning the effects of the generation of heat within such openings nor of the leakage of materials from such openings back to the biosphere.

Salt formations have generally been preferred as candidates for deep geological disposal for a number of reasons (National Research Council, 1957). The relatively high thermal conduction of salt facilitates the dissipation of heat released by the radioactive decay of nuclear wastes. The viscous plasticity of salt, particularly at elevated temperatures, assures that the excavation within which the wastes are disposed will, in the long term, seal themselves by deformation of the salt itself, and the presence of the salt attests to very slow dissolution and transport by movement of groundwater.

However, other geological media may be equally or even better suited for construction of deep underground repositories for nuclear wastes, provided that the openings and access ways to the repository can be sealed adequately. The permeability of intact pieces of many crystalline and argillaceous rocks is at least as low as that of salt. However, the permeability of masses of such rocks arises mainly from the hydraulic conductivity of joints and fractures pervading them, but may still be sufficiently small to retard the movement of groundwater between the repository and the biosphere to an adequate degree.

The purpose of this paper is to study three important aspects concerning the design and performance of such underground repositories for the disposal of nuclear wastes in hard rock. First, the heat released by the radioactive decay of the nuclear wastes causes changes in the spatial and temporal distributions of temperature in the rock mass within which the repository is located. These changes in temperature produce thermally induced components of compressive stress in the heated portions of this rock mass and tensile components of stress outside of this zone. These thermally induced changes in stress may effect the performance and design of a repository. The distribution of temperatures around a repository is necessary to evaluate the thermally induced changes in stress. However, the evaluation of the stress changes is not part of this paper. Second, the magnitude and temporal changes of the temperatures in the rock mass within which the repository is located are affected by the kind of waste and the time after removal from the reactor at which it is buried. The characteristics of different wastes on the temporal changes in temperature are examined. Finally, changes in the temperature of the groundwater in the rock mass containing the repository affect both

the density and viscosity of the water significantly. These changes in density and viscosity may result in perturbations of the original hydrological flow, which could affect the performance of the repository in isolating toxic components of the wastes from the biosphere. A model of buoyant groundwater flow through a simple fracture system is used to assess the magnitude of this phenomenon.

TEMPERATURE FIELD

Repository Model

To study the long term regional changes in temperature in the rock mass the repository is idealized to be a flat circular disk loaded uniformly with nuclear waste at time t=0. The repository is assumed to be a depth, D, of 500 m below surface in granite and to have a radius, R, of 1500 m. The principal mode of heat transfer from the nuclear waste to the rock mass is assumed to be by linear heat conduction. This has been proved to be a good assumption based on recent Stripa data analysis (Hood, 1979).

The temperature field, $T(r,z,t)$, resulting from heat conduction in the rock mass as a function of space and time is given by a solution to the diffusion equation:

$$\frac{1}{r} \frac{\partial}{\partial r} \left(r \frac{\partial T}{\partial r} \right) + \frac{\partial^2 T}{\partial z^2} = \frac{1}{\kappa_T} \frac{\partial T}{\partial t} \tag{1}$$

$$\kappa_T = K/\rho_R C_R ,$$

where r = the radial coordinate;

   z = the axial depth below surface;

   t = the time after loading;

   κ_T = the thermal diffusivity;

   K = the thermal conductivity;

   ρ_R = the density of the rock; and

   C_R = the specific heat of the rock.

Values for the thermal properties of granite and other hard rocks are given in Table 1.

By integrating the solution for an instantaneous point source of heat

over the radius of the repository, R, in the plane z = -D (Carslaw and

Jaeger, 1959), the unit strength of an instantaneous disk heat source can

be found:

$$V_{-D}(r,z,t) = \frac{1}{4(\pi\kappa_T^3 t^3)^{1/2}} \int_0^R \exp\left[-\frac{r^2+r'^2+(z+D)^2}{4\kappa_T t}\right] I_0\left(\frac{rr'}{2\kappa_T t}\right) r'dr', \quad (2)$$

where I_0 is the zeroth order modified Bessel function of the first

kind. When heat is released from the nuclear waste at an average rate

$\phi(t')$ by the disk like repository from time $t' = 0$ to time $t' = t$, the

temperature change at any point (r,z) is:

$$\Delta T(r,z,t) = \frac{1}{\rho_R C_R} \int_0^t \phi(t')V_{-D}(r,z,t-t')dt'$$

$$-\frac{1}{\rho_R C_R} \int_0^t \phi(t')V_{+D}(r,z,t-t')dt' \quad (3)$$

The first term in this equation represents the change in temperature from

the disk-like source in the infinite medium and the second term is a

correction for the presence of a boundary at constant temperature at the

ground surface, z=0.

For the purposes of this paper, equations (2) and (3) have been

solved numerically for a number of expressions $\phi(t')$.

Temperatures on the z-axis for simple functions $\phi(t')$, such as

constant power, exponential decay of power, and a decrease in power

inversely of the square root of time can be expressed in terms of tabula-

ted functions. These are given in Table 2 and can be used to check

the accuracy of the numerical solutions to equations (2) and (3). In

this paper, numerical results reproduces these analytical solutions to

within 0.01°C.

Different Forms of Waste

At present, consideration is being given to the disposal of two principal forms of nuclear waste generally known as high level waste. They are spent fuel, as discharged from a reactor, and the products from reprocessing spent fuel to recover the uranium and plutonium. Assuming that either form of high level waste is buried 10 years after discharge from the reactor, at an initial loading density in the repository of 10 W/m^2, the power densities (Kisner et al., 1978) of the two principal waste forms in the plane of the repository, and of their main constituents, as a function of time are as illustrated in Figure 1. The curves in this figure give, numerically, $\phi(t')$ used in Equation (3). They were used to calculate the changes in temperature in the rock mass containing the repository as described above. Examples of these changes in temperature and isotherms for a repository containing spent fuel or reprocessed waste 100 years and 1000 years after burial in the repository are as illustrated in Figures 2 and 3. It is important to note how much greater are the magnitudes of these changes for spent fuel than for reprocessed waste, especially after 1000 years of burial.

The maximum average temperature in a repository arises at its center and is plotted as a function of time after burial in Figure 4. For both spent fuel and reprocessed waste this temperature reaches a maximum after a period of less than 100 years and thereafter decays very slowly over a period of many thousands of years. The maximum temperature and all other temperatures are of course proportional to the power density with which the repository is loaded.

To study the far field effects and, in particular, those at the surface, the maximum ground surface temperature gradient at the epicenter

above the repository has been calculated for both forms of waste and is as illustrated in Figure 5. This gradient and the corresponding heat flow through the surface reach maximum values at about 2400 years after burial and 1300 years after burial for the spent fuel and reprocessed waste,respectively. The maximum value of the temperature gradient for the spent fuel ,70°C/km, is about three times greater than that of the reprocessed waste ,22°C/km. The total thermal gradient is of course the sum of the original geothermal gradient, typically of 30°C/km, and the thermal gradient induced by the repository.

The power output of various waste forms as a function of time, $\phi(t')$, in a log-log plot can be approximated by segments of straight lines over periods of time after discharge from the reactor. Values of the maximum changes in temperature at the center of the repository as a function of time, and of the epicentral thermal gradient have been calculated for functions of $\phi(t')$ in which power varies inversely as time after discharge from a reactor to the power $\varepsilon = 1$, 2/3 and 1/2, as well as for $\phi(t')$ representing the power output of spent fuel as illustrated in Figure 1. The results of these calculations are as shown in Figure 6. In Figure 7, similar results for reprocessed waste are shown together with those for inverse square root power in time of storage and for an exponential decay of power output with a half life of 30 years. From this figure it can be seen that, because the output of the two principal forms of nuclear wastes decays with time faster than that corresponding to inverse square root, the maximum temperature in any repository must reach a peak value and then decays, such as that illustrated in Figure 4.

The decay in power output of nuclear wastes as a function of time is

determined by their composition and age; different fuel cycles yield wastes with different compositions. To evaluate some of these effects it has been assumed that the repository is loaded with 0.01 $MTHM/m^2$ which is equivalent to a total load in the repository of 0.71×10^6 MTHM. (MTHM = metric ton of uranium fuel charged to the reactors). The maximum temperatures and epicentral thermal gradients as a function of time for different wastes from pressurized water reactor (PWR) and boiling water reactor (BWR) are given in Table 3. The same data are illustrated in Figure 8 for periods of cooling of 10 years after discharge from the reactor. In Table 3, data are also given for a repository loaded at an initial power density of 10 W/m^2.

It can be seen that the differences in temperature for the different fuel cycles arise mainly from the variations of initial power loading density. Even at a constant power loading density 10 W/m^2, significant differences can be seen.

Near Surface Cooling before Emplacement

The power output of all nuclear wastes decays very rapidly immediately after discharge from the reactor. Accordingly, the effects of a period of near surface cooling of these wastes before burial in a repository may be expected to be significant. The effects over short periods of near surface cooling on spent fuel and reprocessed waste for PWR (with initial loading densities of 0.01 $MTHM/m^2$ and 10 W/m^2) on the maximum repository temperatures and epicentral thermal gradients have been calculated and are given in Table 4. The effects of periods of near surface cooling on the maximum repository temperatures and epicentral thermal gradients as a function of time are also illustrated in Figure 9. From these data, it must be concluded that the period for which the wastes are cooled near surface before burial is an important factor in

determining the effect of a repository on the temperatures in the rock mass within which it is located.

Repository Depth and Radius

The effects of different repository depths and radii have been analyzed for situations where the ratio of depth to radius is less than 1. The results are as illustrated in Figure 10. The maximum temperature is not likely to be affected by this range of depths and radii, but changes in far-field, long-term temperatures must be expected. In particular, the epicentral thermal gradient changes with the ratio of the depth of repository below surface to its radius as illustrated in Figure 10.

Rock Properties

The properties of typical hard rocks have been given in Table 1. Using these values the maximum repository temperature and the epicentral thermal gradient have been calculated for a repository loaded with spent fuel or reprocessed waste and the results are as illustrated in Figure 11. From this figure, it can be seen that significant changes in these parameters result from the different rock properties.

THERMOHYDRAULIC EFFECTS

Fracture Flow Model

Changes in the temperature of the rock mass containing a repository will change the temprature of the groundwater in this rock mass. Increasing the groundwater temperature results in decreased density and viscosity of the water. In this section changes in buoyant groundwater flow induced by these temperature changes are evaluated.

The model used for this purpose comprises a simple horizontal fracture at the depth of the repository connecting a recharge zone to a

discharge zone and intersecting a vertical fracture containing the axis

of the repository as is illustrated in Figure 12. Flow from the repository

to the surface occurs through the vertical fracture. The effective

hydraulic aperture of the horizontal fracture is b_x and its permeability

$k_x = b_x^2/12$ (Lamb, 1932; Snow, 1965; Iwai, 1977). The aperture and

permeability of the vertical fracture are b_z and $k_z = b_z^2/12$,

respectively. The flow of groundwater is confined within these fractures.

In practice, the flow of groundwater through most hard rock, which

generally has very low intrinsic permeability (Brace et al., 1968), is

largely through fractures, so that this model approximates the mechanics

of groundwater flow through hard rock masses, differing only in its

simplicity.

Before the repository is loaded and the rock mass subjected to

changes in temperature, it is assumed that the original groundwater flow

is horizontal from recharge zone to discharge zone. As the rock mass

heats up so will the groundwater in the vertical fracture containing the

center of the repository. This will perturb the original flow pattern.

Flow Equations

For any temperature field, the flow of the groundwater must satisfy

the equations of conservation of mass and momentum. The equation

for the conservation of mass is:

$$\frac{\partial \rho}{\partial t} + \nabla \cdot \vec{q} = 0, \qquad (4)$$

where $\vec{q}$ = the mass flux that is the product of the density and velocity

of the water in the fracture;

ρ = density of water; and

t = time.

For low velocities, inertial forces are much less than viscous

forces, so that by means of Darcy's law the equation of momentum can be written as:

$$\nabla P + \frac{\nu}{k} \vec{q} - \rho \vec{g} = 0, \tag{5}$$

where P = pressure;

  ν = kinematic viscosity of water;

  k = permeability; and

  $\vec{g}$ = the gravitational acceleration.

In most studies of thermal convection, because of the small compressibility of water, it is usual to make use of the Boussinesq approximation (Wooding, 1957; Combarnous and Bories, 1975) that variations in the density of water with time can be neglected except for the effects on the buoyancy of the groundwater. As a result of this, equation (4) reduces to:

$$\nabla \cdot \vec{q} = 0, \tag{6}$$

Equations (5) and (6) describe the incompressible flow of groundwater.

The expression $q_z(t)$ for the simple case with zero regional groundwater flow and the repository located a distance, L, midway between the recharge and discharge zones is considered first. The flow is symmetric about x = 0,

$$P(t) = 0, \text{ at } x = 0, z = 0, \tag{7}$$

$$b_x q_x(t) + \tfrac{1}{2} b_z q_z(t) = 0, \text{ at } x = 0, z = -D \tag{8}$$

$$P(t) = P_0 = \int_{-D}^{0} \rho_0(z) g dz, \text{ at } x = L, z = -D \tag{9}$$

Equation (8) describes Kirchoff's Law for the junction between vertical and horizontal fractures. The hydrostatic pressure at the depth z = -D with a water table at z = 0 is P_0. Before loading the repository and heating of the rock mass, the temperature, $T_0(z)$, as a function of depth

may be given by $T_o(z) = (20-0.03z)^\circ C$, where a surface temperature of 20°C and a normal geothermal gradient of 30°C/km is assumed. By imposing a constant pressure boundary condition in equation (9) at the inlet of the horizontal fracture, it is assumed that the temperature at the recharge and discharge zones are not affected by the thermal loading of the repository. This corresponds to recharge and discharge zones far from the repository or with large heat capacities. The contrast in density between the heated water near the repository and the cooled water in the recharge and discharge zone drives the buoyant groundwater flow in the vertical fracture. The limiting case with zero distance from the repository to the recharge and the discharge zone, $L = 0$, is an unrealistic representation of the hydrologic condition of a repository.

In accordance with equation (6), the groundwater flows are independent of the spatial coordinates along the fractures. With constant flow, equation (5) can be integrated from the repository center to the boundary:

$$0 - P(0,-D,t) = -\frac{q_z(t)}{k_z} \int_{-D}^{0} v(0,z,t)\, dz - \int_{-D}^{0} \rho(0,z,t)\, g dz, \tag{10}$$

$$P_o - P(0,-D,t) = -\frac{q_x(t)}{k_x} \int_{0}^{L} v(x,-D,t)\, dx. \tag{11}$$

Equations (8), (10), (11) can be solved for the unknowns $q_z(t)$, $q_x(t)$ and $P_o(0,-D,t)$. The result for $q_z(t)$ is:

$$q_z(t) = \left[\frac{k_z \rho_o(0) g}{v_o(0)}\right] \left[\frac{\Delta h_b(t)}{\bar{D}(t)}\right] \left[\frac{2b_x k_x/\bar{L}(t)}{2b_x k_x/\bar{L}(t)+b_z k_z/\bar{D}(t)}\right], \tag{12}$$

where

$$\Delta h_b(t) = \int_{-D}^{0} \frac{\rho(x,z,t) - \rho_o(z)}{\rho_o(0)}\, dz; \tag{13}$$

$$\bar{L}(t) = \int_{0}^{L} \frac{v(x,-D,t)}{v_o(0)}\, dx; \tag{14}$$

$$\overline{D}(t) = \int_{-D}^{0} \frac{\nu(p,z,t)}{\nu_o(0)} \, dz. \tag{15}$$

The factors $\Delta h_b(t)$, $\overline{L}(t)$, and $\overline{D}(t)$ have the definition of lengths and can be referred to as effective hydraulic heads. Equation (12) is a product of three factors. The first of these is the hydraulic conductivity of the vertical fracture; the second, the gradient resulting from buoyancy and the last, a correction for the hydraulic resistance of the horizontal fracture between the recharge and discharge zone and the repository. The product of the last two factors is an effective vertical hydraulic gradient, $(\nabla h)_z$. From equation (13), $q_z(t)$ can be evaluated by the numerical integration of the effective heads, equations (13)-(15). Values for density, $\rho(x,z,t)$ and viscosity $\nu(x,z,t)$ are calculated at the temperature $T_o(z) + \Delta T(x,z,t)$. Values for $\rho_o(z)$ and $\nu_o(z)$ are calculated at $T_o(z)$ (Meyer et al.1967).

To calculate the displacement of water in the vertical fracture, $q_z(t)$ can be integrated over time. Before loading the repository and heating the rock mass the total amount of static water inside the vertical fracture per unit width is:

$$M_o = b_z \int_{-D}^{0} \rho_o(z) dz. \tag{16}$$

After heating the rock mass, $q_z(t) \neq 0$, and the cumulative amount of water flow across a given horizontal section is:

$$M(t) = b_z \int_{0}^{t} q_z(t') dt' \tag{17}$$

Water initially at a level $z = -D$ moves upward to a depth given by

$$Z(t) = -D(1 - M(t)/M_o),$$ (18)

for $M(t) \leq M_o$. The vertical displacement $Z(t)$ results from the buoyancy of the water in the vertical fracture.

Equation (12) for $q_z(t)$ can be generalized to the case when $q_o \neq 0$, $L_{rc} \neq L_{dc}$ where the subscripts rc and dc refer, respectively, to recharge and discharge zones. If the original groundwater flow is not zero, the hydraulic heads at the recharge and discharge zones, h_{rc}, h_{dc} must be different. The pressure difference between the recharge and discharge zones is:

$$\Delta P_o = \int_{h_{dc}}^{h_{rc}} \rho_o(z) \, g \, dz \cong \rho_o(0) \, g(h_{rc} - h_{dc}).$$ (19)

From equation (5) the flow in horizontal fracture at the depth $z = -D$ is:

$$q_o = -\frac{k_x \rho_o(0) g}{\nu_o(-D)} (\nabla h)_o$$

where (20)

$$(\nabla h)_o = \frac{h_{rc} - h_{dc}}{h_{rc} + h_{dc}}$$

represents the hydraulic gradient between these zones. The use of the density of water at surface $\rho_o(0)$ and a subsurface viscosity $\nu_o(-D)$ in the equation for the flow q_o is an artifact of this model where water is driven through a horizontal fracture by difference in the near surface water tables.

To drive $q_z(t)$ for $q_o \neq 0$ and $L_{rc} \neq L_{dc}$, $2b_x q_x$ in equation (8) must be replaced by $b_x(q_{rc}(t) - q_{dc}(t))$. The pressure boundary condition in equation (9) is replaced by two equations with the upper limit of the integral set as h_{rc} or h_{dc} instead of zero, and Darcy's equation is integrated over both horizontal lengths $x > 0$ and $x < 0$. The expression for $q_z(t)$ is:

$$q_z(t) = \left[\frac{b_x k_x k_z \rho_o(0) g}{\nu_o(o)}\right]\left[\frac{\Delta h_b(t)(1/\bar{L}_{rc}(t) + 1/\bar{L}_{dc}(t)) + (\nabla h)_o(L_{rc}/\bar{L}_{rc}(t) - L_{dc}/\bar{L}_{dc}(t))}{b_z k_z + b_x k_x \bar{D}(t)(1/\bar{L}_{rc}(t) + 1/\bar{L}_{dc}(t))}\right] \quad (21)$$

Note that equation (21) reduces to Equation (12) for $L_{rc} = L_{dc}$, even when $(\nabla h)_o \neq 0$ or $q_o \neq 0$. That is, the buoyant flow in the vertical fracture is independent of the flow in the horizontal fracture for the symmetric case.

Results of Buoyant Flow

Consider first the case where the vertical and horzontal fractures have the same aperture $b_z = b_x = 1$ μm, with a repository radius of 1500 m and a length to the recharge and discharge source L = 5000 m. Groundwater initially at the depth of the repository will move upward in a vertical fracture as a function of time after the emplacement of the wastes. The results of a repository at a depth of 500 m and a depth of 1000 m are plotted in Figure 13. The buoyancey and the movement of groundwater is proportional to the change in temperature of the rock mass as can be seen by comparison with Figure 3. The vertical flow in the case of spent fuel is substantially greater than is that for reprocessed waste. There is little difference due to the change in depth. Essentially the flow of water as a result of buoyancy depends upon the average temperature of the groundwater throughout the length of the vertical fracture.

In addition to the buoyancy of the heated water in the vertical fracture, the flow of this water is affected by the hydrologic connection between the recharge and discharge zones represented by the horizontal fracture. The shorter the distance from the repository to recharge zone the greater will be the flow of water in the vertical

fracture for a given buoyancy. As examples, the velocities have been calculated for distances between the repository and recharge zone at L = 0, 2000 m, 5000 m, 10,000 m and the results are as illustrated in Figure 14 for repository depths of 500 m and 1000 m (L = 0 is an unrealistic limiting case). The most important factor affecting the buoyant flow of groundwater is the ratio between the distance L from repository to the recharge zone and the depth D of the repository.

From equation (12) or equation (21), if the hydraulic resistances of the horizontal fracture were infinite (b_x = 0 or L = ∞), buoyant flow in the vertical fracture could not occur. For the general realistic case with finite constant values of b_x ($b_x \neq 0$, $b_x \neq \infty$) and L (L $\neq$ 0, L = ∞), q(t) does not become infinite as b_z increases. On the contrary, $q_z(t)$ approaches zero as b_z corresponds to ∞, that is, a large vertical fracture with storage capacity reduces buoyant flow. It can be shown that $q_z(t)$ as a maximum value with $b_z = (4\bar{D}(t)/\bar{L}(t))^{1/3}b_x$, and

$$q_z(t) \leq \frac{1}{3}\left[\frac{k_x\rho_o(0)g}{\nu_o(0)}\right]\left[\frac{\Delta h_b(t)}{\bar{D}(t)}\right]\left[\frac{4\bar{D}(t)}{\bar{L}(t)}\right]^{2/3} \tag{22}$$

Buoyant groundwater flow in the vertical fracture has an upper bound which is determined by the permeability of the horizontal fracture rather than the permeability of a vertical fracture. In Figure 15 results with a constant aperture b_x = 1 μm and with a range of apertures b_z = 10 μm, 1 μm and 0.1 μm are illustrated. The movement of the groundwater in the vertical fracture is significantly slower both for the case of b_z = 10b_x and b_z = 0.1b_x than with b_z = b_x. The finite recharge capacity through the horizontal fracture restricts the vertical buoyant flow.

All the preceeding results have been calculated for the symmetrical
situation. In Figure 16 the effects on the buoyant flow of groundwater
in the vertical fracture of the position of the repository between
the recharge and discharge zones is illustrated. Finally the effect
of different original geothermal gradients on buoyant groundwater flow in
the vertical fracture has been analyzed as shown in Figure 17 for spent
fuel and reprocessed waste. The buoyant flow of groundwater in the
vertical fracture decreases slightly as the original geothermal gradient
increases.

DISCUSSION

Although the thermo-hydrolgoic model used for the analysis presented in this paper is very simple, it should possess the same physical behavior as that of the more complex systems of fractures which account for the permeability of masses of hard rock. Accordingly, it should provide a good insight into the dynamics of thermally-induced groundwater flow, and illustrate the sensitivity of this flow to various parameters. However, the actual numerical results should be considered as no more than an order of magnitude estimations. It must be pointed out also that the transport of nuclides from the repository to surface does not take place at the same rate as that of the groundwater. Nuclide transport is retarded in a certain degree as results of physical and chemical processes, such as sorption.

The calculations reported in this paper suggest that, under certain circumstances, thermally-induced buoyant groundwater flow may be a mechanism by which toxic materials from a repository could be transported to the biosphere. The magnitude of this flow depends upon many factors. Of these, the aggregate increase in the temperature of the rock mass containing the repository is one of the most important. This temperature is affected by the design of the repository, the kind of nuclear waste buried in it and the period for which this waste has been cooled near surface before burial. Significant differences exist between reprocessed waste and spent fuel in respect of the degree to which the rock mass is heated and hence the time taken for groundwater to reach the surface by buoyant flow. The depth of the repository below surface is of much less significance. Cooling of the wastes near surface can be used to compensate for these differences and reduce substantially the total amount of heat put into the rock mass. The heat capacity of different kinds of

rocks has a significant effect on buoyant groundwater flow also. Finally, the buoyant groundwater flow depends upon the ratio of the hydraulic transmissivities of the vertical and horizontal fractures, the maximum flow being determined by the transmissivity of the horizontal fracture.

REFERENCES

Brace, W.F., J.B. Walsh., and W.T. Frangos, Permeability of granite under high pressure: J. Geophys. Res., 73, no. 6, pp. 2225-2236, 1968.

Carslaw, H.S., and J.C. Jaeger, Conduction of heat in solids; Oxford at the Clarendon Press, 2nd ed., p. 260, 1959.

Combarnous, M.A. and S.A. Bories, Hydrothermal convection in saturated porous media, Adv. in Hydroscience, 10, pp. 231-307, edited by V.T. Chow, Academic Press, Inc., New York, 1975.

Department of Energy, Report of task force for review of nuclear waste management, DOE/ER-0004/D, UC-70, Washington, D.C., U.S. Department of Energy, Directorate of Energy Research, February 1978.

Fairchild, P.D., G.D. Brunton and J.F. Cuderman, National waste terminal storage program on radioactive waste storage; Program progress report, Y/OWI-8, Office of Waste Isolation, Oak Ridge National Laboratory, Oak Ridge, Tennessee, p. 133, November 1976.

Hood, M., Some results from a field investigation of thermo-mechanical loading of a rock mass when heater canisters are emplaced in the rock, presented at the 20th U.S. Symposium on Rock Mechanics, Austin, Texas, June 4-6, 1979.

Interagency Review Group on Nuclear Waste Management, Subground report on alternative technology strategies for the isolation of nuclear waste, TID-28818, October 1978.

Iwai, K., Fundamental studies of fluid flow through a simple fracture, Ph.D. Thesis, University of California, Berkeley, 1977.

Kappelmeyer, O., and R. Haenel, Geothermics with special reference to application, Geopublication Associates, Berlin, Stuttgart, 1974.

Kisner, R.A., J.R. Marshall, D.W. Turner, and J.E. Vath, Nuclear waste projections and source-term data for FY 1977, Y/OWI/TM-34, Office of Waste Isolation, Oak Ridge National Laboratory, Oak Ridge, Tennessee, April 1978.

Lamb, H., Hydrodynamics, Cambridge University Press, New York, 6th Edition, p. 583, 1932.

Martinez-Baez, L.F. and C.H. Amick, Thermal properties of Gable Mountain basalt cores, Hanford Nuclear Reservation, LBL-7038, Lawrence Berkeley Laboratory, Berkeley, California, 1978.

Meyer, C.A., R.B. McClintock, G.J. Silvestri, and R.C. Spencer, Jr., 1967 ASME steam tables; The American Society of Mechanical Engineers, New York, New York, 1967.

National Research Council, The disposal of radioactive waste on land, Committee on Waste Disposal, Division of Earth Sciences, National Academy of Sciences, Washington, D.C., 1957.

Pratt, H.R., T.A. Schrauf, L.A. Bills, and W.A. Hustralid, Thermal and mechanical properties of granite, Stripa, Sweden; TR-77-92, Terra Tek, Salt Lake City, Utah, October 1977.

Snow, D.T., A parallel-plate model of permeable fractured media, Ph.D. Thesis, University of California, Berkeley, California, 1965.

Wooding, R.A., Steady free thermal convecting of liquid in a saturated permeable medium, J. Fluid Mech. 2, pp. 273-285, 1957.

Table 1

Thermal Properties of Rocks

Rock	K (W/m/°C)	R (kg/m^3)	C_R (J/kg/°C)	κ_T (10^{-6}m^2/sec)
Granite[*]	2.5	2600	836	1.15
Stripa- Granite[†]	3.2	2600	837.36	1.47
Basalt[‡]	1.62	2865	1164	0.486
Shale[§]	0.90	2300	1000	0.391

[*]Kappelmeyer and Haenel, 1974
[†]Pratt, et al.,1977
[‡]Martinez-Baez and Amick, 1978
[§]Fairchild et al.,1976

Table 2

Analytic Solutions of Temperature Rise
on the z-axis of Disk Source

Power form	Power density $\phi(t)$	Solution form* $f(x,t)$
Constant	$\phi(0)$	$\dfrac{\phi(0)(\kappa_T t)^{\frac{1}{2}}}{K}$ ierfc (x)
Exponential decay	$\phi(0) \exp(-\lambda t)$	$\dfrac{\phi(0)}{K} (\kappa_T/\lambda)^{\frac{1}{2}}$ ImW$[(\lambda t)^{\frac{1}{2}} + ix]$
Inverse Square Root	$2 T_o K/(\pi\kappa_T t)^{\frac{1}{2}}$	T_o erfc(x)

$*\ \Delta T(0,z,t) = f\{[(z+D)^2/4\kappa_T t]^{\frac{1}{2}}, t\} - f\{[(R^2 + (z+D)^2)/4\kappa_T t]^{\frac{1}{2}}, t\}$

$-f\{[(z-D)^2/4\kappa_T t]^{\frac{1}{2}}, t\} + f\{[(R^2 + (z-D)^2)/4\kappa_T t]^{\frac{1}{2}}, t\}$

ierfc = first integral of complementary error function

erfc = complementary error function

ImW = imaginary part of the error function of complex argument

Table 3

Effects of Fuel Cycles

Nuclear reactor	Fuel-cycle	$(\Delta T)_{max}$ * $^\circ C$	$(\Delta(\nabla T)_z)_{max}$ * $^\circ C/km$	Power density at loading* W/m^2	kW/canister
PWR	Spent fuel	60 (50)	83 (70)	11.9 (10)	.548
	HLW+PuO$_2$: U-recycle	65 (52)	86 (69)	12.5 (10)	2.61
	HLW : U+Pu recycle	90 (40)	68 (30)	22.7 (10)	4.75
	HLW : U-recycle	43 (42)	22 (22)	10.2 (10)	2.14
	HLW: no recycle	43 (41)	22 (22)	10.3 (10)	2.16
BWR	Spent fuel	50 (51)	73 (74)	9.96 (10)	.182
	HLW+PuO$_2$: U-recycle	57 (54)	77 (73)	10.5 (10)	2.20
	HLW : U+Pu recycle	71 (40)	59 (34)	17.5 (10)	3.65
	HLW : U-recycle	35 (42)	19 (23)	8.30 (10)	1.74
	HLW: no recycle	35 (42)	19 (23)	8.35 (10)	1.75

$(\Delta T)_{max}$: Maximun value of the average temperature rise at the center of repository.

$(\Delta(\nabla T)_z)_{max}$: Maximun value of the ground surface thermal gradient rise at the epicenter above the repository.

* Values without parenthesis correspond to 0.01 MTHM/m^2 waste capacity.

Values with parenthesis correspond to 10 W/m^2 power density.

Table 4

Effects of Surface Cooling

Waste form	Surface cooling[†] period (year)	$(\Delta T)_{max}$[*] $^{\circ}C$	$(\Delta(\nabla T)_z)_{max}$[*] $^{\circ}C/km$	Power density at loading[*] W/m^2	kW/canister
Spent fuel of PWR	1	98 (9)	93 (9)	104. (10)	4.81
	2	76 (14)	90 (16)	56.4 (10)	2.60
	5	67 (33)	86 (43)	20.1 (10)	.927
	10	60 (50)	83 (70)	11.9 (10)	.548
Reprocessed HLW: no recycle of PWR	1	95 (9)	35 (3)	103. (10)	21.5
	2	62 (11)	31 (6)	55.0 (10)	11.5
	5	50 (27)	26 (14)	18.7 (10)	3.9
	10	43 (41)	22 (22)	10.3 (10)	2.16

$(\Delta T)_{max}$: Maximun value of the average temperature rise at the center of repository.

$(\Delta(\nabla T)_z)_{max}$: Maximun value of the ground surface thermal gradient rise at the epicenter above the repository.

* Values without parenthesis correspond to 0.01 $MTHM/m^2$ waste capacity.

  Values with parenthesis correspond to 10 W/m^2 power density.

† Spent fuel - fuel assembly discharge directly from the reactor.

  $HLW + PuO_2$: U-recycle - reprocessed waste with U and Pu removed from the discharge fuel, U recycled in the reactor, and Pu stored together with the waste.

  HLW : U+Pu recycle - reprocessed waste with U and Pu removed from the discharge fuel and recycled in the mixed oxide reactor.

  HLW : U-recycle - reprocessed waste with U and Pu removed from the discharge fuel and U recycled in the reactor.

  HLW : no-recycle - reprocessed waste with U and Pu removed from the discharge fuel.

Figure 1: Areal power densities of spent fuel and reprocessed high level waste versus time after discharge from a pressurized water reactor. The power densities are normalized to 10 W/m^2 at 10 years after discharge when the wastes are assumed to be stored in a respository. The wastes contain the short-lived fission products and the long-lived actinides. In the reprocessed waste, 99.5% of the actinides U and Pu are removed.

Figure 2: Temperature rise contours around repository after 100 years of waste storage and the corresponding temperature profiles along the vertical axis through the center of the repository and along the radial axis in the plane of the repository. The repository, in granite with 500 m in depth and 1500 m in radius, is stored with either spent fuel or reprocessed waste at initial loading density of 10 W/m^2 at 10 years after discharge from PWR.

Figure 3: Temperature rise contours around repository after 1000 vears of waste storage and the corresponding temperature profiles along the vertical axis through the center of the repository and along the radial axis in the plane of the repository. The repository, in granite with 500 m in depth and 1500 m in radius, is stored with either spent fuel or reprocessed waste at initial loading density of 10 W/m^2 at 10 years after discharge from PWR.

Figure 4: Temperature rise ΔT at the center of repository versus storage time. The repository, in granite with 500 m in depth and 1500 m in radius, is stored with either spent fuel or reprocessed waste at initial loading density of 10 W/m^2 at 10 years after discharge from PWR.

Figure 5: Ground surface temperature gradient rise $\Delta(\nabla T)_z$ and heat flux rise $\Delta(K(\nabla T)_z)$ (in HFU = $\mu cal/cm^2/sec$) at the epicenter above the repository. The repository, in granite with 500 m in depth and 1500 m in radius, is stored with either spent fuel or reprocessed waste at initial loading density of 10 W/m^2 at 10 years after discharge from PWR.

Figure 6: Repository center's temperature and ground surface epicentral thermal gradient versus storage time of spent fuel are compared with the results calculated with power denisities varying inversely as time after discharge to the power $\varepsilon = 1$, 2/3 and 1/2 (log-log straight lines passing through 10 W/m^2 and 10 years after discharge in Figure 1). The repository is in granite with 500 m in depth and 1500 m in radius.

Figure 7: Repository center's temperature and ground surface epicentral thermal gradient versus storage time of reprocessed waste are compared with the results calculated with the power density varying exponentially with 30 years half-life and with the power density varying inversely as square root in storage time with initial temperature of 40°C. The repository is in granite with 500 m in depth and 1500 m in radius.

Figure 8: Effects of different fuel cycles on the repository center's temperature and ground surface epicentral thermal gradient versus storage time. The wastes of different fuel cycles are: (1) spent fuel — fuel assembly discharge directly from the reactor; (2) HLW : no-recycle — reprocessed waste with U and Pu removed from the discharge fuel; (3) HLW + PuO_2 : U-recycle — reprocessed waste with U and Pu removed, U recycled in the reactor, and Pu stored together with reprocessed waste; (4) HLW : U+Pu recycle — reprocessed waste with U and Pu removed from the discharge fuel and recycled in the mixed oxide reactor. The repository, in granite with 500 m in depth and 1500 m in radius, is stored with 0.01 $MTHM/m^2$ of wastes at 10 years after discharge from PWR.

Figure 9: Effects of different surface cooling periods of wastes after discharge from reactor and before burial in repository on the repository center's temperature and ground surface epicentral thermal gradient versus storage time. The repository, in granite with 500 m in depth and 1500 m in radius, is stored with 0.01 $MTHM/m^2$ of spent fuel or reprocessed waste of PWR.

Figure 10: Effects of different depths and radii of repository on the ground surface epicentral thermal gradient versus storage time. The repository in granite is stored with either spent fuel or reprocessed waste at initial loading density of 10 W/m^2 at 10 years after discharge from PWR.

Figure 11:   Effects of different rock formations on the repository center's temperature and ground surface epicentral thermal gradient versus storage time.   The repository, with 500 m in depth and 1500 m in radius, is stored with either spent fuel or reprocessed waste at initial loading density of 10 W/m^2 at 10 years after discharge from PWR.

Figure 12:   Two fracture model for simulating groundwater movement through a repository located between the recharge and discharge zone. The thermal loading at the repository induces the buoyant flow along the vertical fracture to the ground surface.   The horizontal fracture (with aprture b_x; and length 2L if the repository is located midway between the recharge and discharge zone) recharges the vertical fracture (with aperture b_z; and length D) to maintain the buoyant flow.

Figure 13:   Water movement along vertical fracture from the repository versus storage time.   The repository depth is either 500 m or 1000 m. The stored waste is either spent fuel or reprocessed waste at initial loading density of 10 W/m^2 at 10 years after discharge from PWR. The repository is in granite with radius of 1500 m and distances to the recharge and discharge zone of 5000 m. Both horizontal and vertical fractures have 1 μm aperture.

Figure 14: Effects of different recharge distances L and repository

depths D on the flow velocities and hydraulic gradients along the

vertical fracture versus storage time. . Both horizontal and vertical

fractures have 1 µm aperture. The repository, in granite with 1500 m

in radius and located midway between the recharge and the discharge

zone, is stored with either spent fuel or reprocessed waste at

intially loading density of 10 W/m^2 at 10 years after discharge from

PWR. The velocities are sensitive to the ratio of the horizontal

distance L to the vertical depth D.

Figure 15: Effects of different vertical fracture apertures b_z on

the water movement along the vertical fracture from the repository

versus storage time. The horizontal fracture aperture b_x is constant

at 1 µm. The repository depth is either 500 m or 1000 m. The stored

waste is spent fuel at initial loading desnity of 10 W/m^2 at 10 years

after discharge from PWR. The repository is in granite with radius of

1500 m and distance to the recharge and discharge zone of 5000 m.

The water movement is significantly slower both for the case of $b_z = 10 \, b_x$

and $b_z = 0.1 \, b_x$ than with $b_z = b_x$.

Figure 16: Effects of different recharge distance L_{rc} and discharge

distance L_{dc} on the water movement along the vertical fracture from

the repository versus storage time. The original horizontal hydraulic

gradient is 0.001 m/m. The repository depth is either 500 m or

1000 m. The stored waste is either spent fuel or reprocessed waste

at initial loading density of 10 W/m^2 at 10 years after discharge from

PWR. The repository is in granite with radius of 1500 m. Both hori-

zontal and vertical fractures have 1 µm aperture.

Figure 17:   Effects of different original geothermal gradient on the water movement along the vertical fracture from the repository versus storage time.   The repository depth is either 500 m or 1000 m.   The stored waste is either spent fuel or reprocessed waste at initial loading density of 10 W/m^2 at 10 years after discharge from PWR. The repository is in granite with radius of 1500 m and distances to the recharge and discharge zone of 5000 m.   Both horizontal and vertical fractures have 1 μm aperture.

Figure 1

XBL 7810-11962

Figure 2

Spent fuel
1000-year storage

Reprocessed HLW
1000-year storage
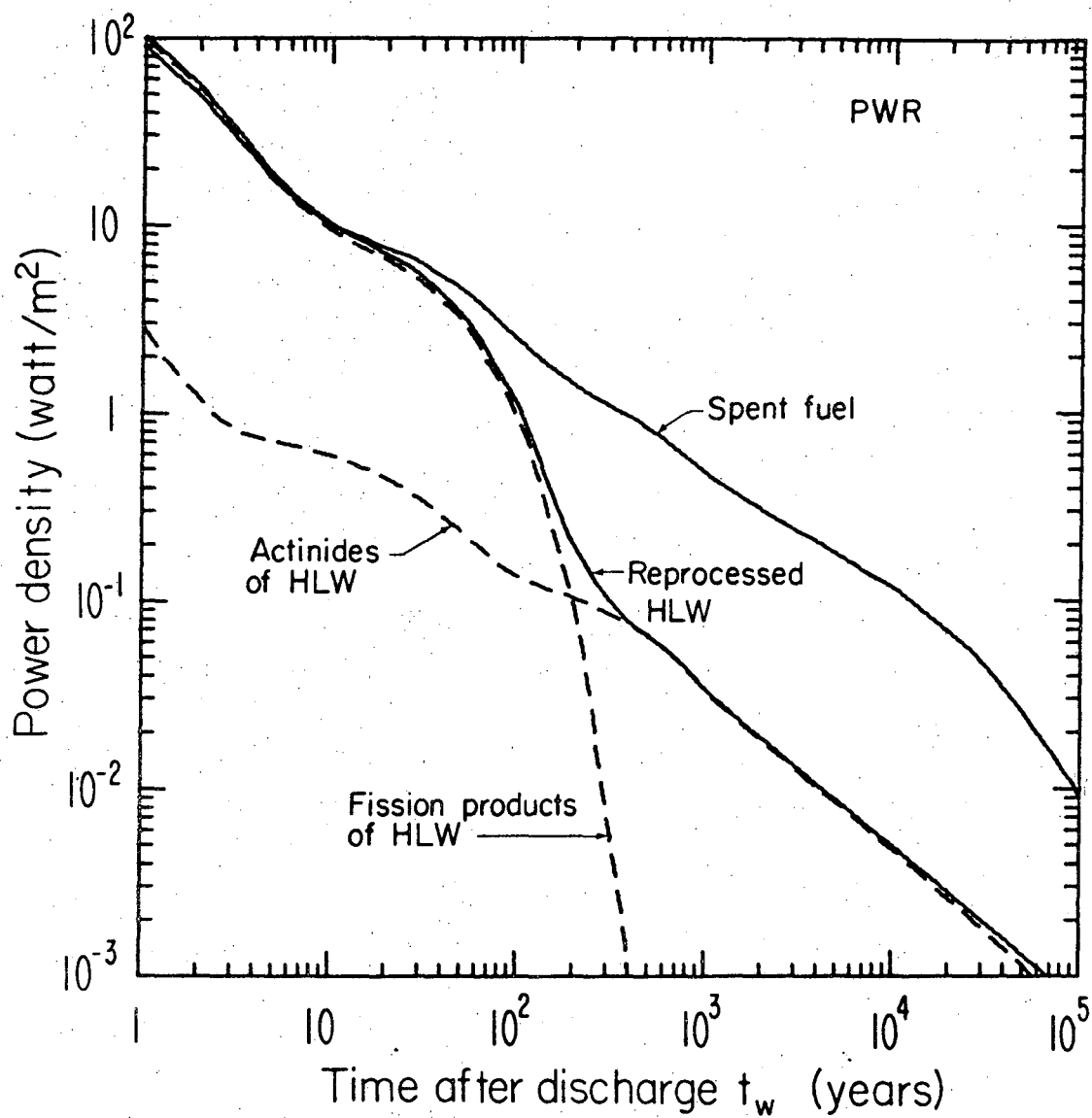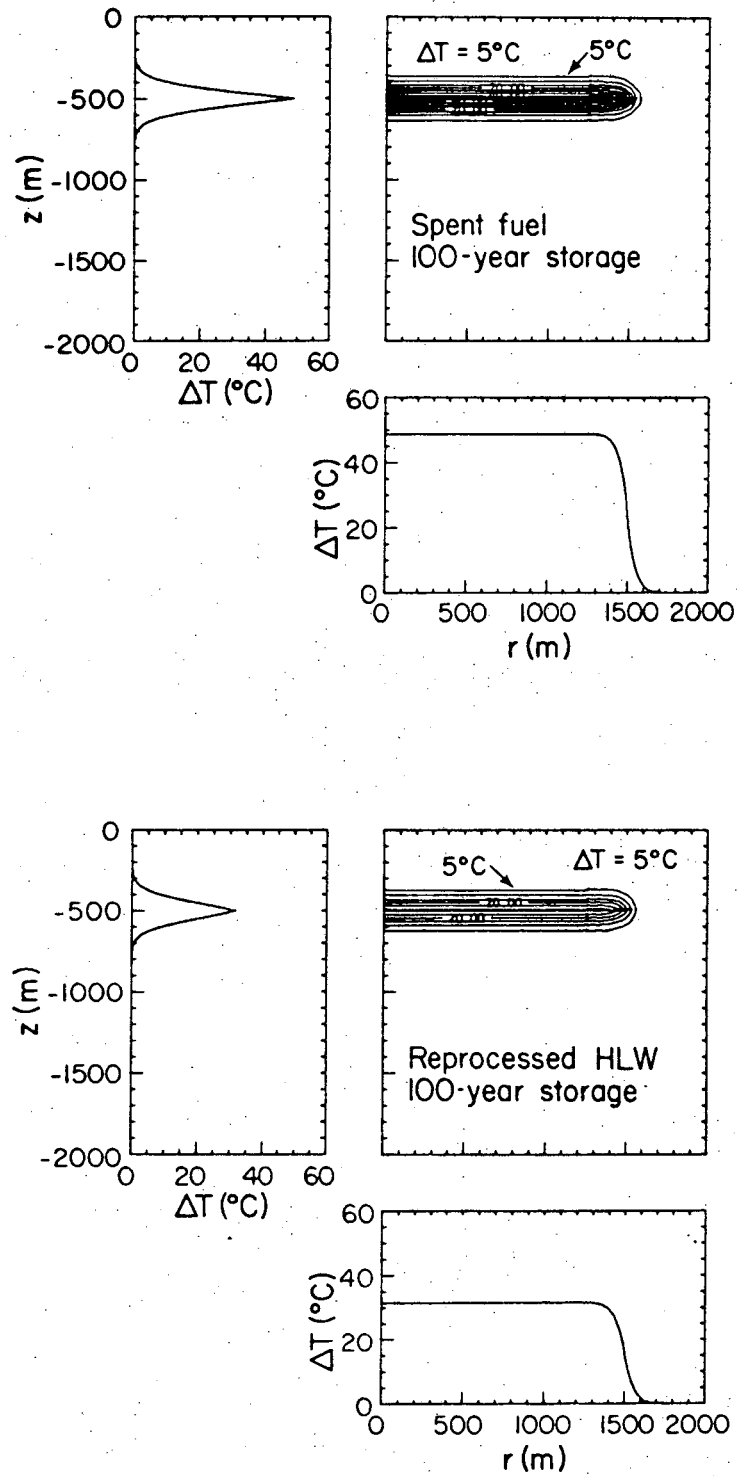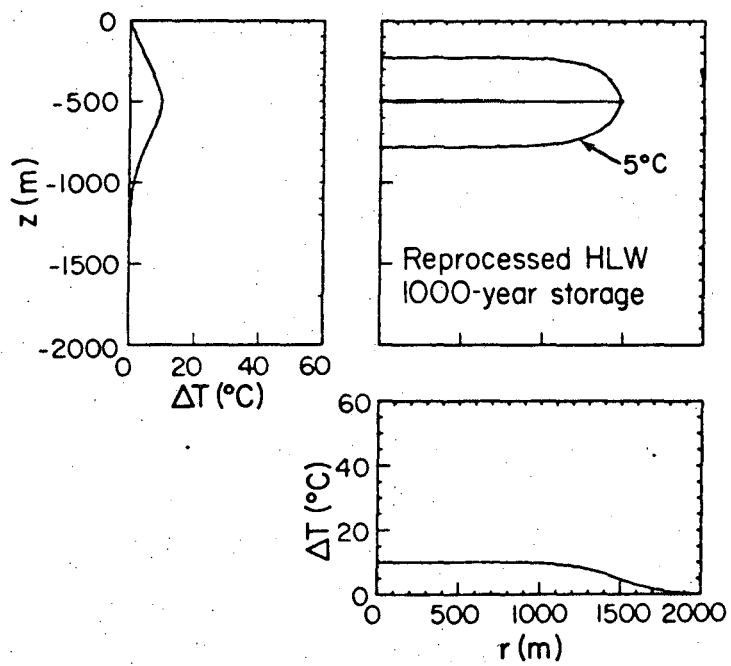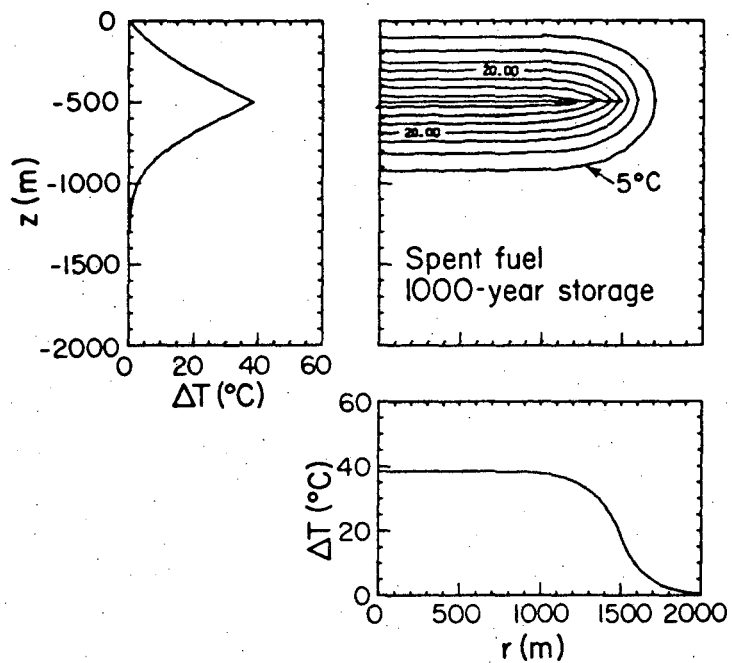
XBL 7810-11957
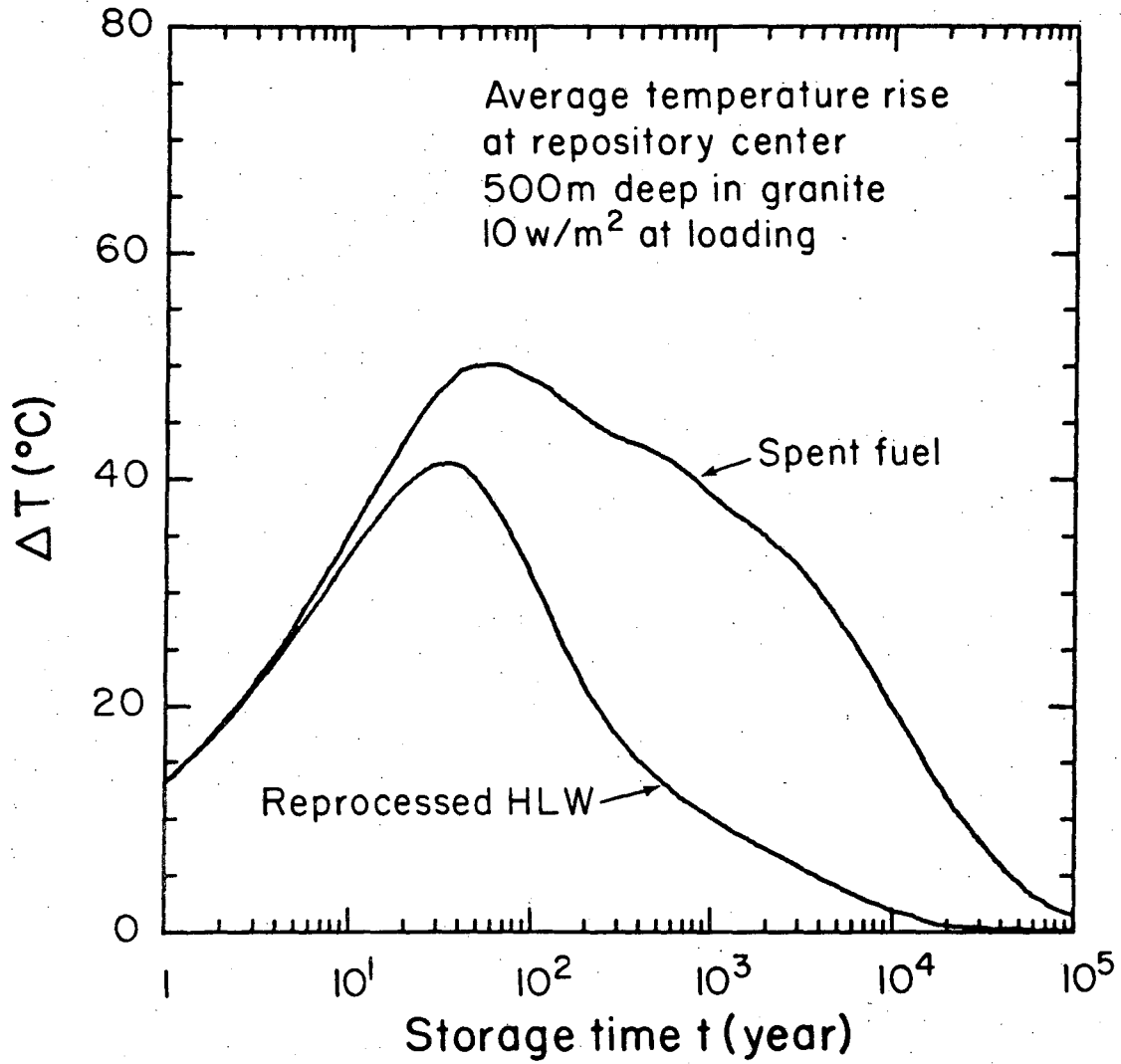
Figure 3

Figure 4

XBL 7810-11951
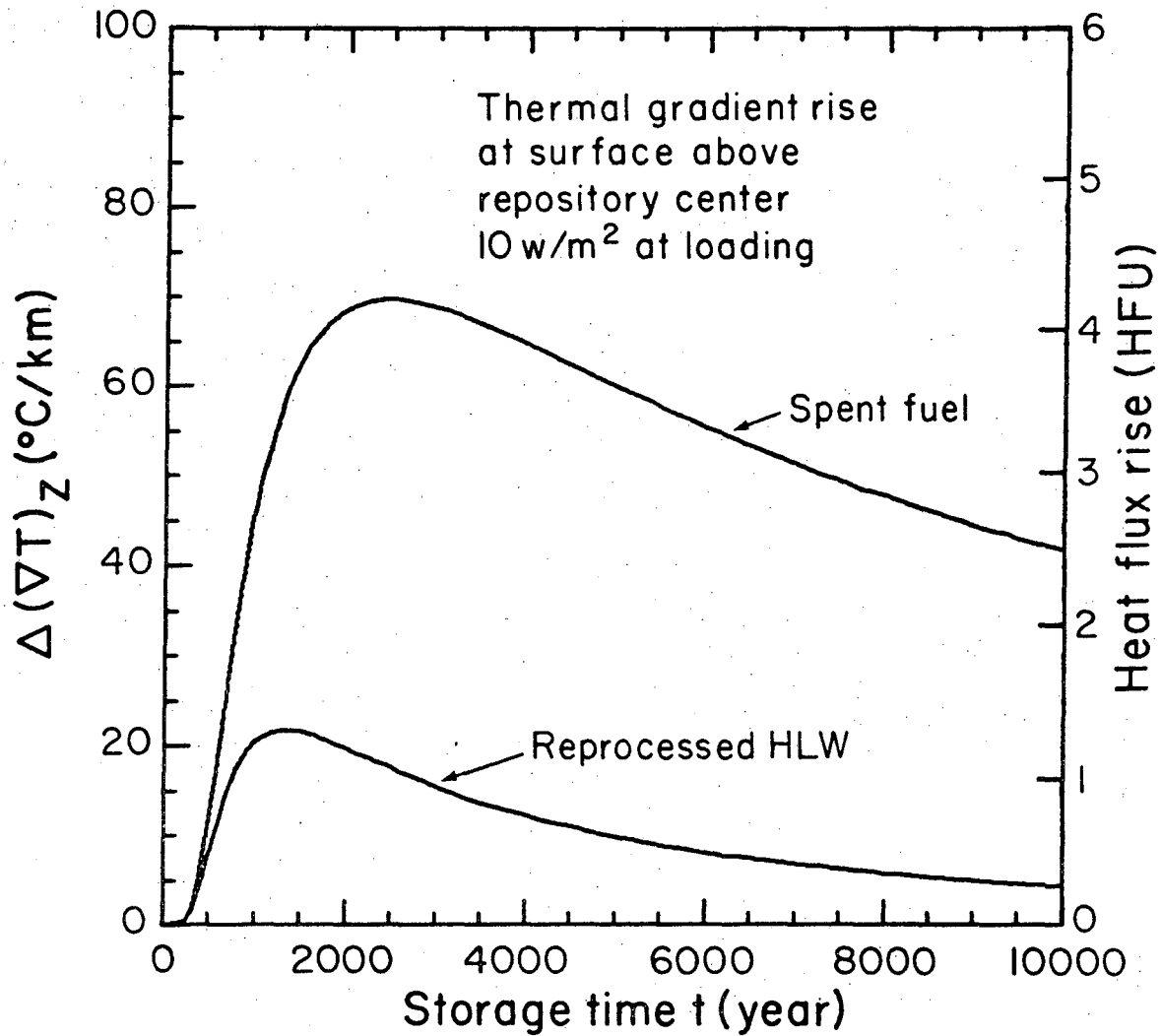
Figure 5
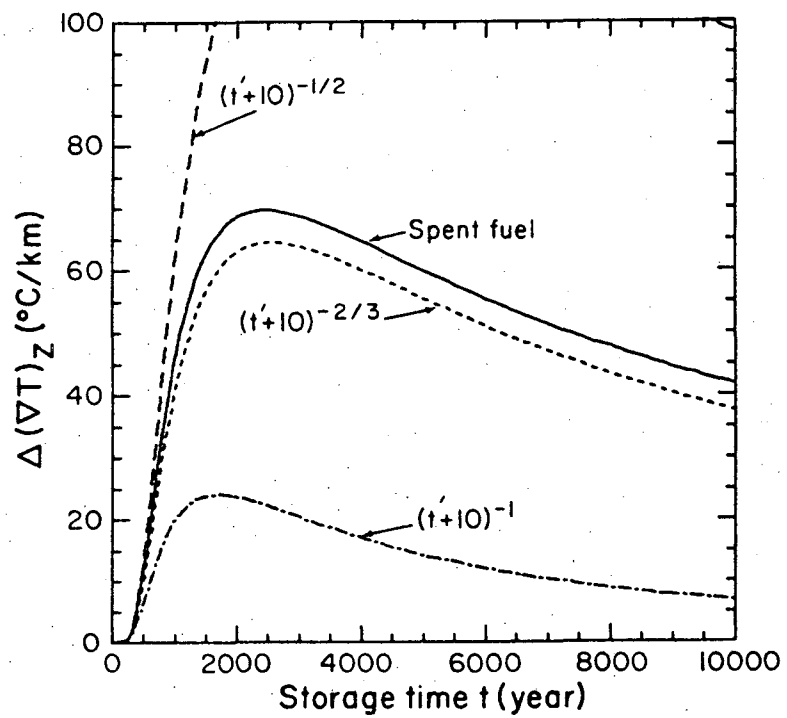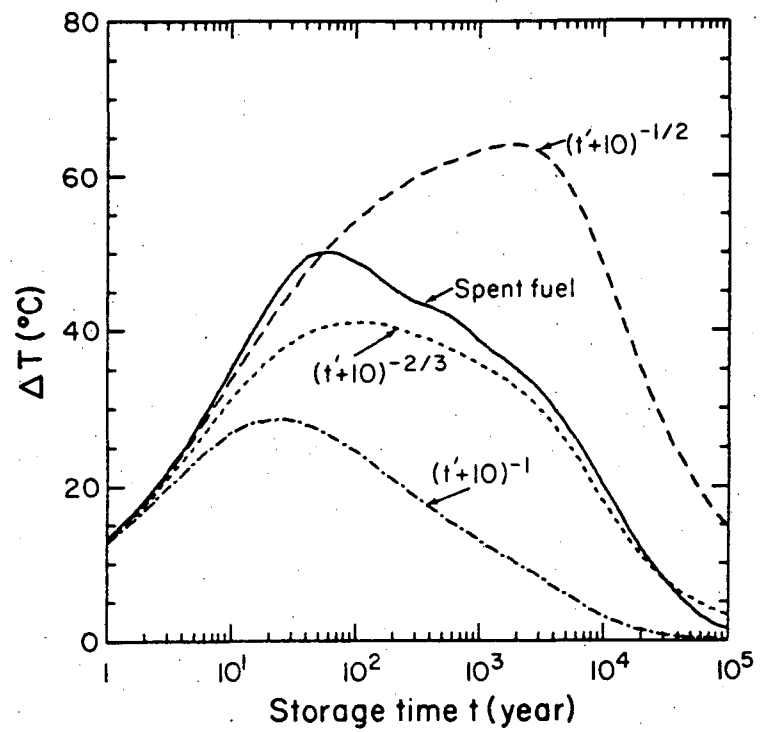
XBL 7810-11952

XBL 7810-11947

Figure 6
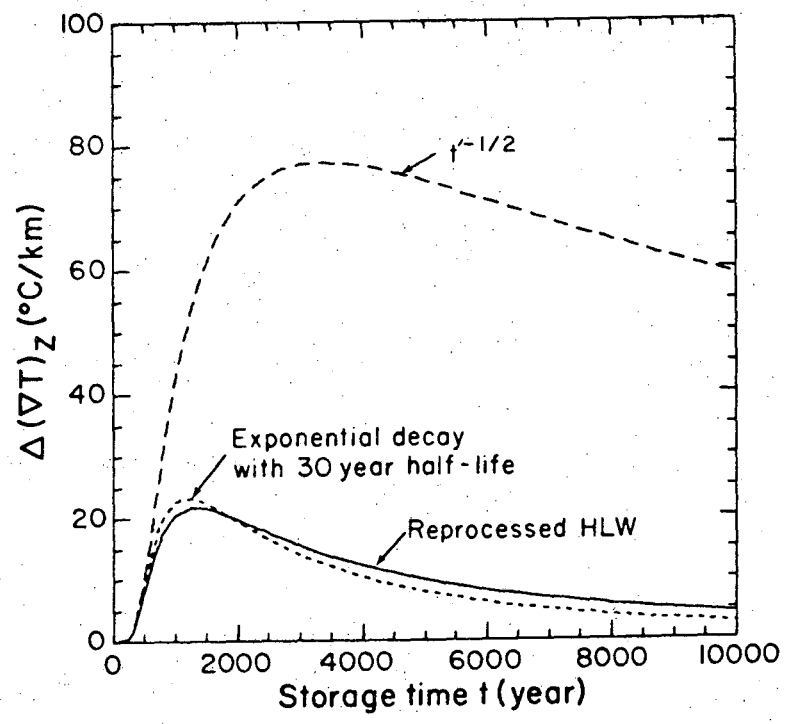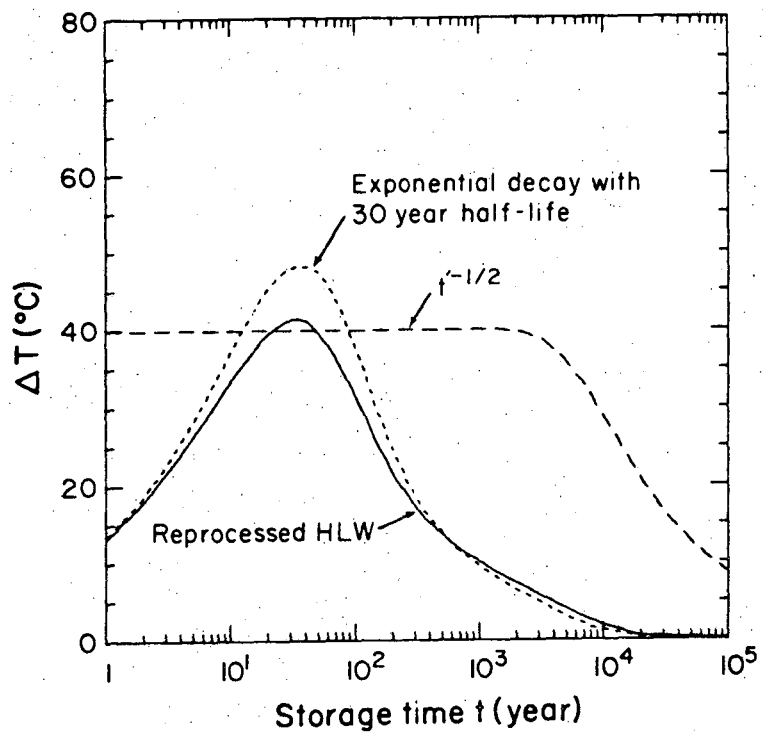
Figure 7

XBL 7810-11945

Figure 8
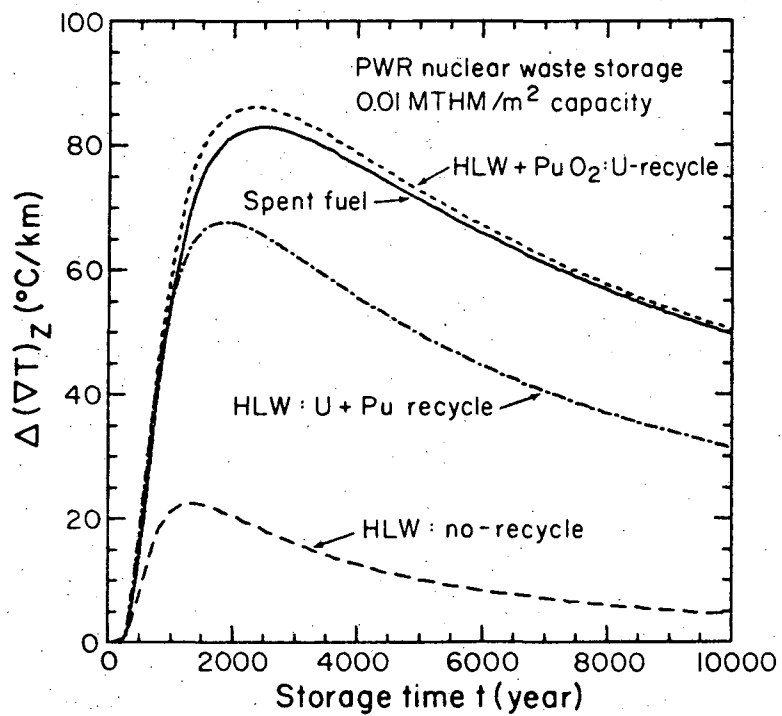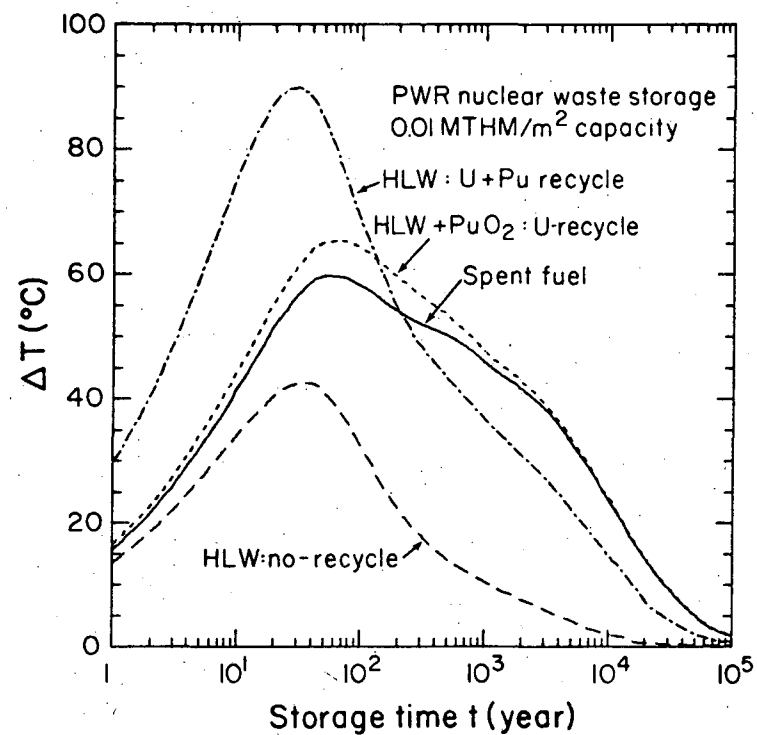
XBL 7810-11942
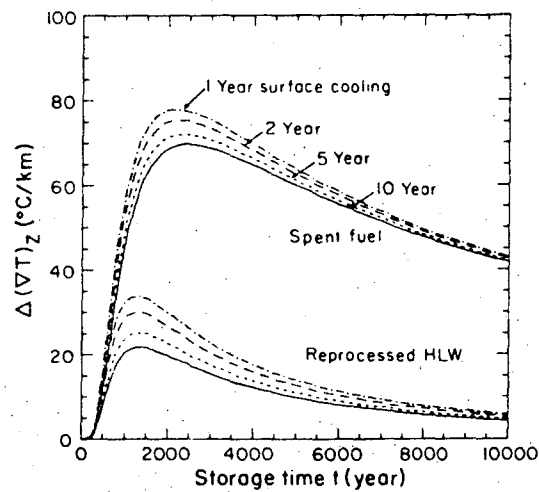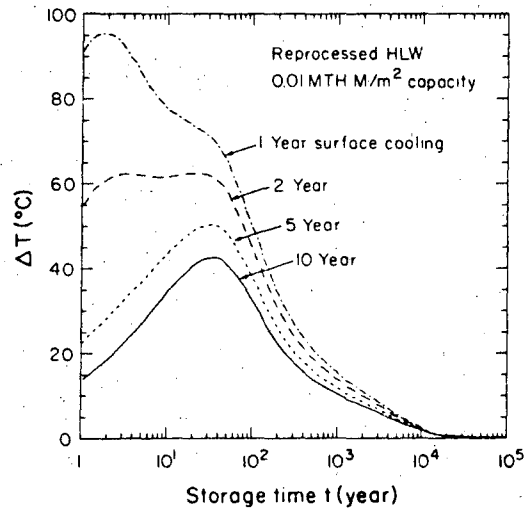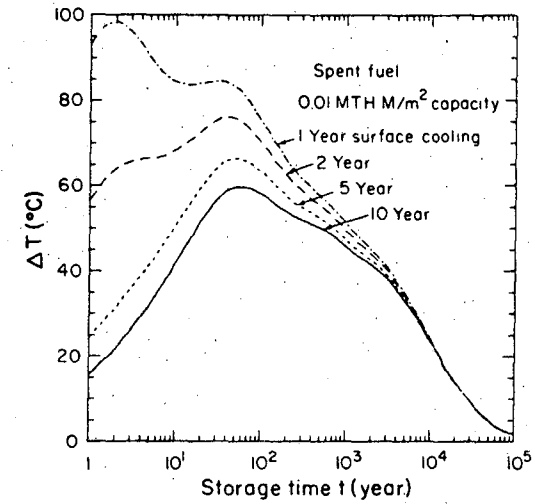
Figure 9
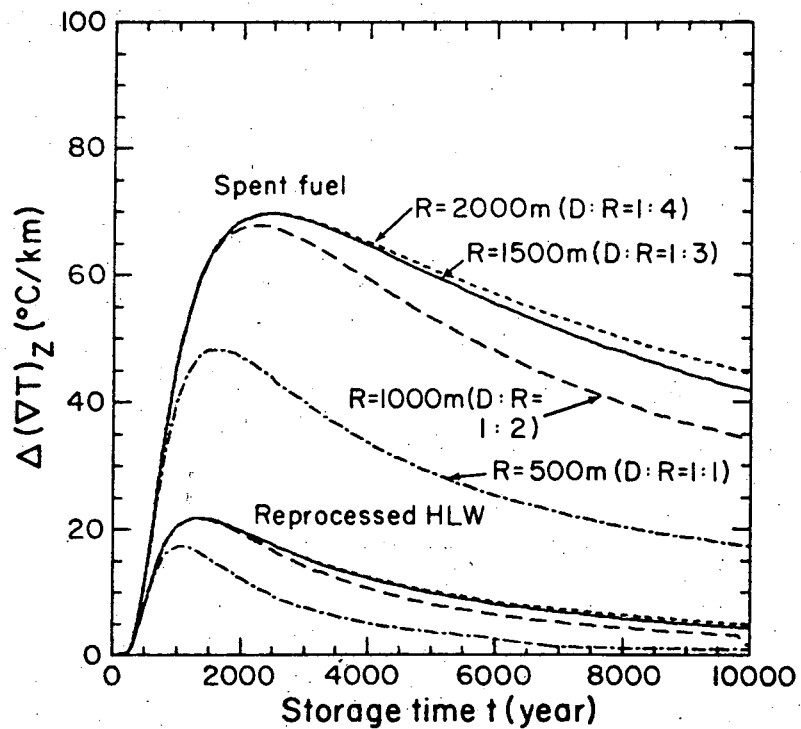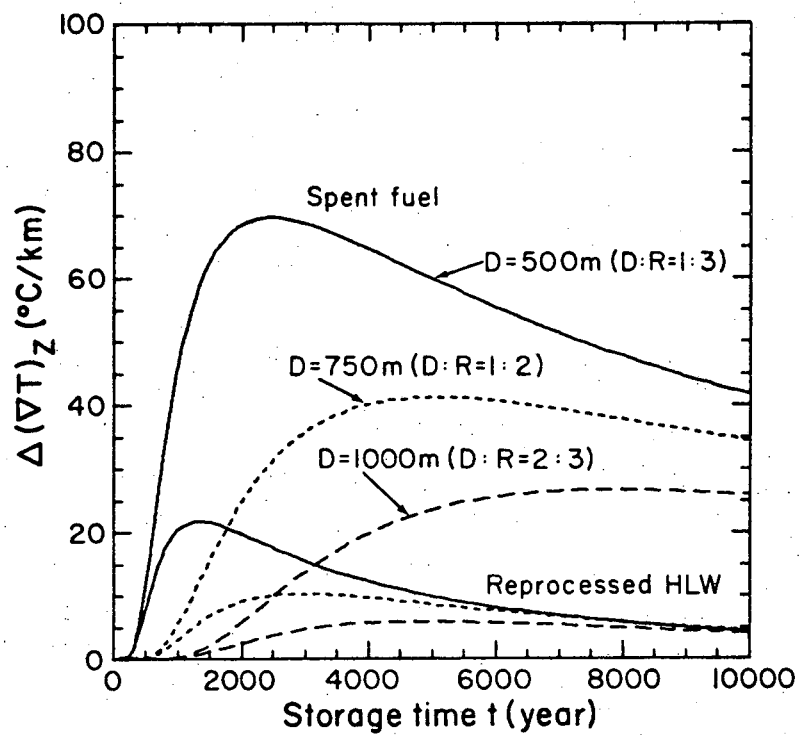
XBL 7810-11950

XBL 7810-11946A

Figure 10

XBL 7810-11948

Figure 11

DISCHARGE
ZONE

RECHARGE
ZONE

REPOSITORY

1 km
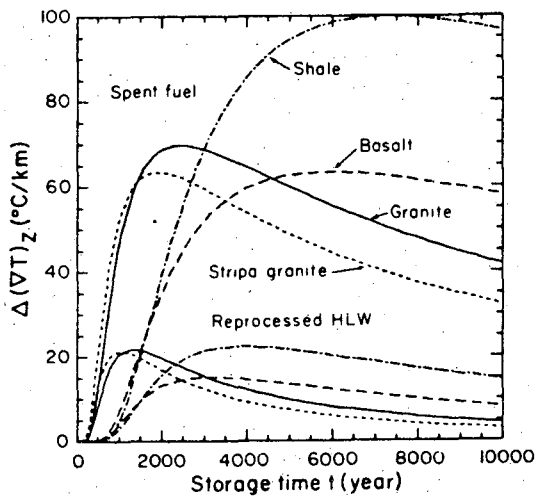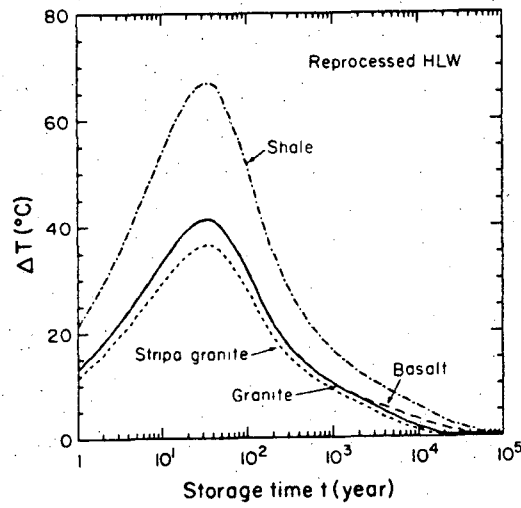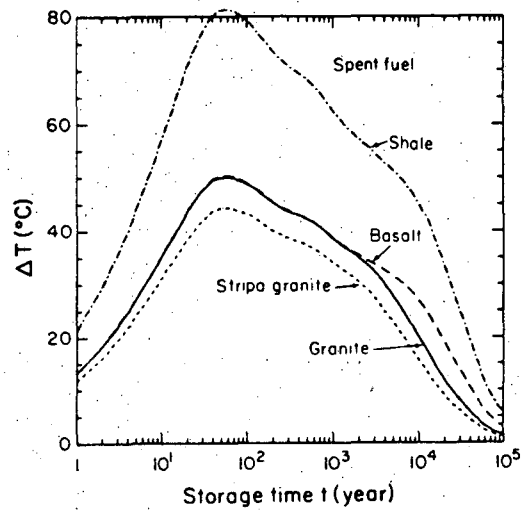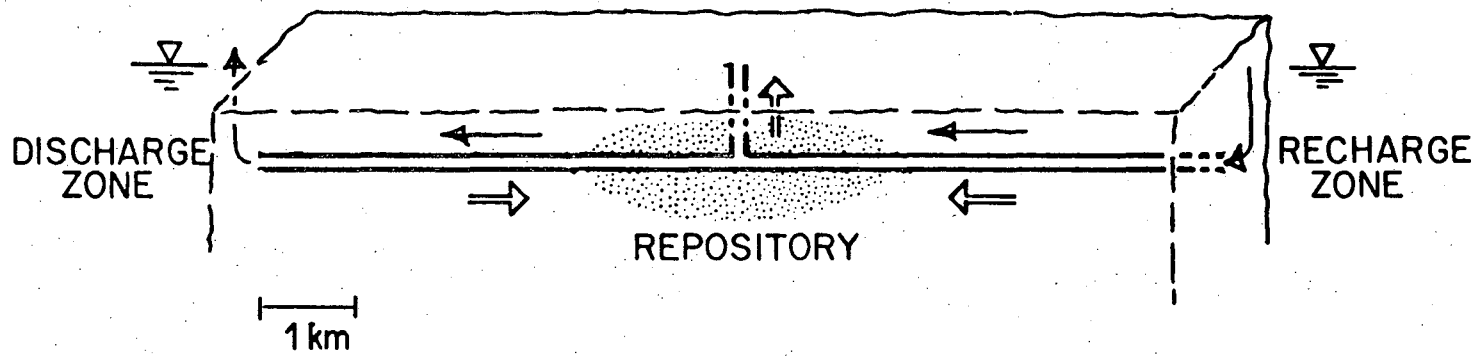
◄— Initial flow

⇐ Induced buoyancy flow

═══ Fractures (not to scale)

Vertical
fracture

b_z

Horizontal
fracture

b_x

Figure 12

XBL 78I0-II678

44
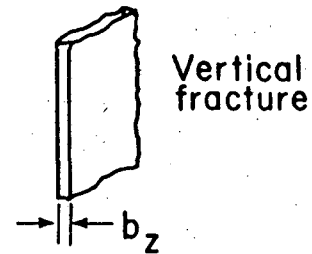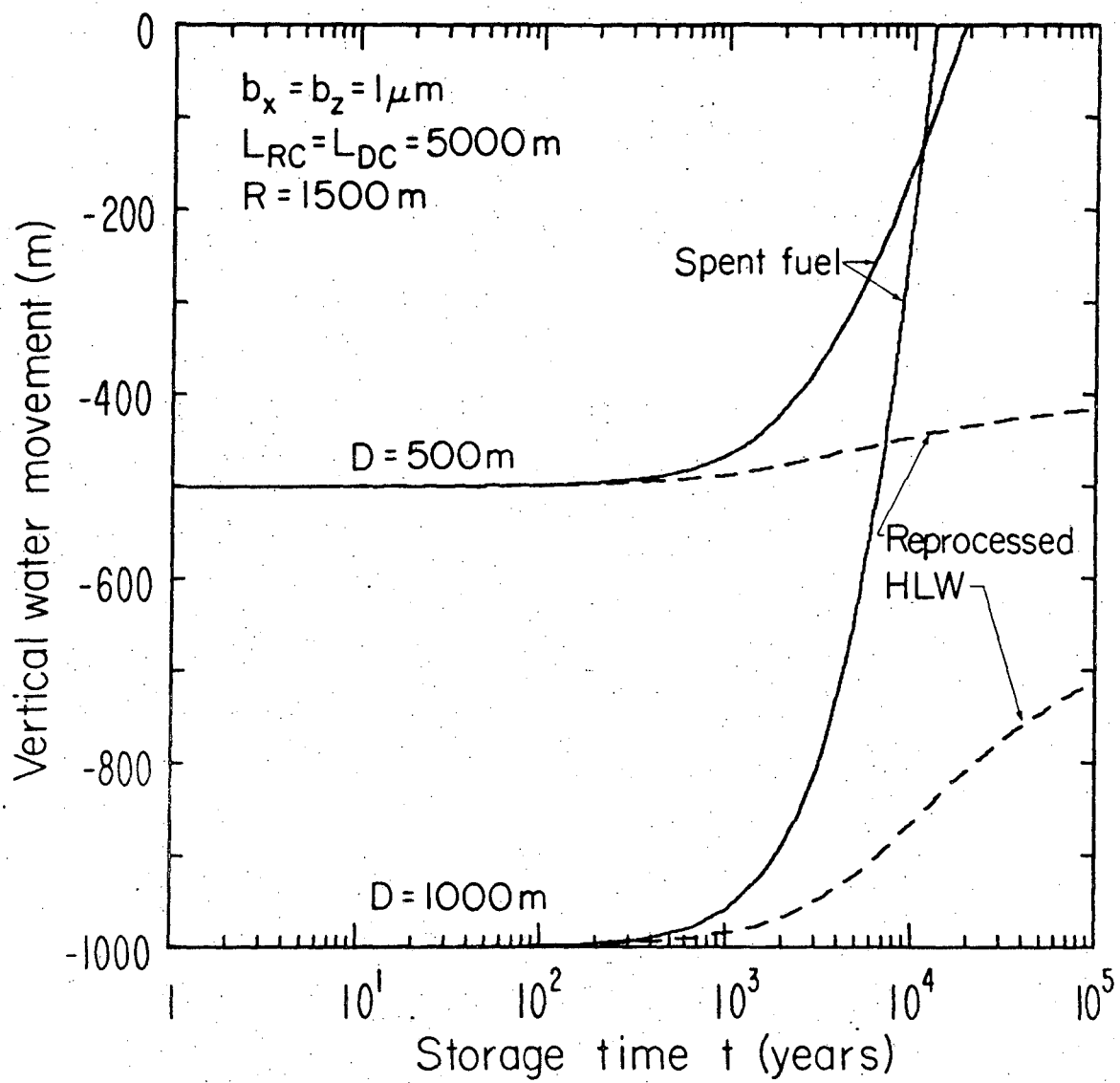
Figure 13

Figure 14

XBL 7812-14033

Figure 15

XBL 7810-11961

Figure 16

XBL 7810-11990

Figure 17

XBL 7810-11989